micromachines

MDPI

Article

Generation of Oil Droplets in a Non-Newtonian Liquid Using a Microfluidic T-Junction

Enrico Chiarello [1], Ladislav Derzsi [1], Matteo Pierno [1], Giampaolo Mistura [1,*] and Evandro Piccin [2]

Received: 28 September 2015; Accepted: 23 November 2015; Published: 30 November 2015
Academic Editors: Andrew deMello and Xavier Casadevall i Solvas

[1] Dipartimento di Fisica e Astronomia "G. Galilei", Università di Padova, via Marzolo 8, 35131 Padova, Italy; enrico.chiarello@gmail.com (E.C.); ladislav.derzsi@unipd.it (L.D.); matteo.pierno@unipd.it (M.P)
[2] Departamento de Química, Universidade Federal de Minas Gerais, Belo Horizonte 31270-901, Brazil; evandrop@ufmg.br
* Correspondence: giampaolo.mistura@unipd.it; Tel.: +39-049-8277020; Fax: +39-049-8277003

Abstract: We have compared the formation of oil drops in Newtonian and non-Newtonian fluids in a T-junction microfluidic device. As Newtonian fluids, we used aqueous solutions of glycerol, while as non-Newtonian fluids we prepared aqueous solutions of xanthan, a stiff rod-like polysaccharide, which exhibit strong shear-thinning effects. In the squeezing regime, the formation of oil droplets in glycerol solutions is found to scale with the ratio of the dispersed flow rate to the continuous one and with the capillary number associated to the continuous phase. Switching to xanthan solutions does not seem to significantly alter the droplet formation process. Any quantitative difference with respect to the Newtonian liquid can be accounted for by a suitable choice of the capillary number, corresponding to an effective xanthan viscosity that depends on the flow rates. We have deduced ample variations in the viscosity, on the order of 10 and more, during normal operation conditions of the T-junction. This allowed estimating the actual shear rates experienced by the xanthan solutions, which go from tens to hundreds of s^{-1}.

Keywords: droplet microfluidics; T-junction; squeezing regime; non-Newtonian fluids; matrix viscoelasticity; xanthan solutions; shear-thinning

1. Introduction

Droplet-based microfluidics is a blossoming research field that presents great potential for high-throughput chemical and biological analysis, synthesis of advanced materials, sample pretreatment, protein crystallization, and encapsulation of cells [1–6]. This technology relies on the production of pico- to nano-liter volume droplets at high throughput rates (typically 1–10 kHz) and with high uniformity. Polydispersity, defined as the standard deviation of the size distribution divided by the mean droplet size, can be as small as 1%. The three most common approaches to produce uniform trains of droplets are [7]: (i) breakup in co-flowing streams, (ii) breakup in elongational- or stretching-dominated flows, and (iii) breakup in cross-flowing streams, as obtained in a T-junction. In general, droplets of a fluid forming the so-called dispersed phase are carried by the stream of a second immiscible fluid identified as the continuous phase. The dynamics of the break-up of the dispersed phase and the formation of drops are relatively well understood in the case of two immiscible Newtonian fluids as, for example water and oil [8–10]. More recently, this investigation has been extended to viscoelastic non-Newtonian liquids in flow-focusing geometries and in T-junctions because of the potential interest in manipulating samples of physiological liquids such as blood, synovial fluid, or saliva. Most of the attention was devoted to the formation of viscoelastic droplets carried by Newtonian continuous phases [11] and the effect of polymer molecular weight

on filament thinning in flow-focusing devices [12,13]. The production of Newtonian droplets in a viscoelastic medium has instead been systematically investigated in the flow-focusing geometry to analyze the focusing effect due to the non-Newtonian continuous phase [14]. It was found that, with careful adjustment of the ratio of viscosities of the two immiscible liquids, viscoelasticity of the focusing liquid could help to lower the dispersion of the emulsions and to decrease the volume of the produced droplets.

Here we focus on the previously never studied case in an experiment of the formation of (Newtonian) oil droplets in a non-Newtonian medium by using T-shaped microchannel junctions. Droplet formation in a T-junction was first reported by Thorsen *et al.* [15], who used pressure controlled flows in microchannels to generate droplets of water in a variety of different oils. More recently, polymeric droplets of low viscosity, elastic fluids were generated in T-junctions [16] (case of droplet viscoelasticity, DV). Dilute aqueous solutions of polyethylene oxide of various molecular weights were used as the droplet phase whilst silicone oils were used as the continuous phase. The effects of viscosity ratio and fluid elasticity on the mechanism of drop detachment and break-up, final drop size and frequency of drop formation were studied. Similar droplet sizes were obtained for similar flow conditions regardless of the nature of the dispersed phase. However, the formation of elongated filaments between subsequent drops was observed only for the non-Newtonian case. Similar filaments between viscoelastic droplets were also observed by Christopher and Anna [17]. Gu and Liow employed xanthan solutions of different concentrations as dispersed phase in a T-junction with various oils used as continuous phase and observed that increasing the viscosity of the dispersed phase resulted in decreasing droplet size for the Newtonian fluids but increasing droplet size for the xanthan solutions [18]. More recently, Li and co-authors [19] studied the characteristics of viscoelastic droplets formed under low interfacial tension in T-junction microchannels. Again, the generated droplets showed distinct morphological characteristics when compared with those produced with Newtonian fluids, with the drop tail streaming composed by tiny satellites at the rear of the droplet. To the best of our knowledge, no other experimental work has been published on the production of non-Newtonian droplets in T-junctions.

Numerical simulations [20] indicate that (for fixed flow conditions) the effects of viscoelasticity are more pronounced in the case of Newtonian droplets in a viscoelastic carrier liquid than in the complementary case of viscoelastic droplets in a Newtonian medium. This difference is quantitatively attributed to the fact that the flow driving the break-up process upstream of the emerging thread can be sensibly perturbed by a viscoelastic behavior of the continuous phase, obtained for example by adding polymers [20]. We thus decided to investigate the viscoelastic effects of the continuous phase on the formation of (Newtonian) droplets. Most non-Newtonian fluids exhibit several viscoelastic properties: notably, concentrated polymer solutions are characterized by both shear-thinning and normal stress effects [21,22]. In order to concentrate on shear-thinning flow properties, we have studied aqueous solutions of xanthan, a stiff rodlike polysaccharide. Xanthan was chosen because it is reported to have a strong shear rate dependence of the viscosity and smaller elastic effects (*i.e.*, normal stresses) [23,24]. Finally, in this preliminary study, we focused on the squeezing regime, where the droplet break-up process is dominated by the pressure drop across the plug as it forms [10].

2. Materials and Methods

2.1. Fabrication

The plan was to use disposable T-junction microfluidic chips to get statistically robust results. Their geometry was chosen to promote squeezing. Thus, the width of the main channel had to be greater than its height and the width of the inlet channel had be at least equal to half the width of the main channel [10], see Figure 1. We started the fabrication using polyester-toner (PeT) devices made by direct-printing combined with xurography because they were shown to be suitable to produce oil-in-water (O/W) droplets without using any surface treatment of the microchannels' walls [25].

Briefly, transparency films (polyester sheets 100 µm thick) were printed twice on both sides using an office laser printer. A knife plotter (Craft Robo CC200-20, Graphtec, Tokyo, Japan) was used to produce the microchannels in small pieces (55 mm × 35 mm) of the printed films. The resulting cut-through printed polyester layer was placed between two unprinted polyester layers, with the upper one provided with access holes. Finally, the three polyester sheets were laminated using an office laminator at 150 °C and the reservoirs were constructed by gluing small pieces of rubber tubes (4 mm of i.d. and 10-mm-long) with epoxy resin. The difficulty in duplicating the microfluidic chips and the partial wetting of the channels walls by the continuous phase made it problematic to get reproducible data.

We then made T-junctions devices in a thiolenic optical adhesive (NOA81 by Norland Products, Inc., Cranbury, NJ, USA) by photolithography and replica molding [26]. A relief mold was fabricated using the negative photoresist SU-8 (MicroChem, Newton, MA, USA) spin coated over a silicon wafer using photolithography. Positive copies in polydimethylsiloxane (PDMS) were replicated using this master. The PDMS pre-polymer and cross-linker (Sylgard 184, Dow Corning, Midland, MI, USA) were mixed in a 10:1 (w/w) ratio and cured at 80 °C for 1 h. The NOA81 resin was then poured over this PDMS master and cured with UV light (365 nm) for about 1 h. The replica was then peeled off from the master and the microchannels were closed by spin coating a microscopic layer of NOA81 over a piece of flexible transparency foil followed by a UV exposition of 1 min. This short exposure was chosen to leave the resin in a semi-cured state. Subsequently, the coated transparency foil and the patterned NOA provided with access holes were brought into contact and exposed to UV light for 30 min. This methodology guarantees a much better control of the microchannels shape [27] with respect to PeT devices, however the wettability of the NOA surface by the continuous phase was not satisfying. The need of adding a surfactant (Triton X-100) to the continuous phase restricted the range of possible aqueous solutions that could be employed due to the limited solubility of the surfactant. Actually, we found that Triton X-100 was not soluble in glycerol/water solutions above 60%. Furthermore, for xanthan solutions, the concentration of the surfactant was comparable to that of the polymer and it is well known that the presence of the surfactant can affect the droplet formation [28].

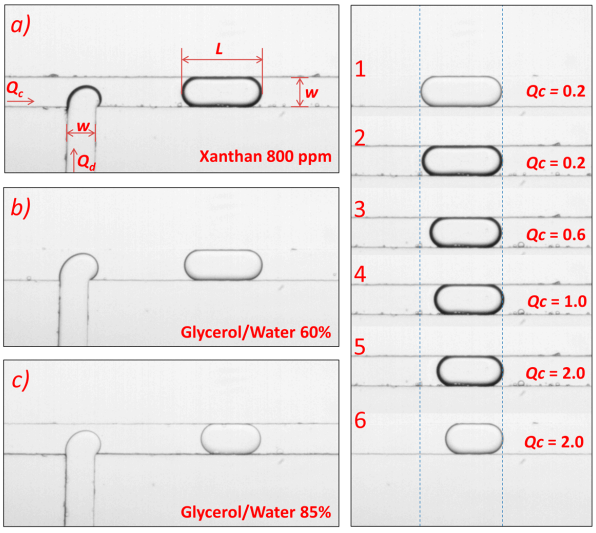

Figure 1. Images (**a**)–(**c**): snapshots of the production of linseed oil droplets in different continuous phases taken at the same flow rate ratio $\phi = 0.5$ and $Q_c = 0.6$ µL/min. The width of the microchannels forming the T-junction device is $w = 120$ µm and their height $h = 90$ µm. Images 1–6: snaphots of linseed droplets in different continuous phases at the same $\phi = 0.5$ and different Q_c measured in µL/min. Images 1 and 6 refer to 60% (w/w) glycerol/water and 2–5 to 800ppm (w/w) xanthan/water solutions as continuous phase.

To overcome such limitations, we switched to microchannels in PDMS whose walls were made hydrophilic after a surface treatment with polyvinylpyrrolidone, PVP (molecular weight, M_w ~40,000 g/mol, Sigma Aldrich, St. Louis, MI, USA). This allowed the generation of oil droplets without the addition of any surfactant to the continuous phase. Briefly, PDMS microfluidic chips were fabricated using standard techniques of photo and soft-lithography. The chip pattern was designed with AutoCAD (Autodesk, Mill Valley, CA, USA) and transferred to transparency-based photomasks using a high-resolution printer. Silicon wafers were spin-coated with the negative photoresist SU-8 (MicroChem) and exposed to UV light through the photomask. After curing the SU-8, the masters were silanized. PDMS pre-polymer and cross-linker were mixed in a ratio of 10:1 (w/w), stirred thoroughly and degassed under vacuum, before being poured onto the SU-8 masters. After curing at 80 °C for 1 h, the PDMS replica was peeled off from the master and irreversibly bonded to a microscope glass slide after an oxygen plasma treatment using a FEMTO Plasma System (Type B, 0–1000 W, Diener Electronic, Ebhausen, Germany) at a power of 300 W for 60 s. Hydrophilic microchannels were obtained by modifying the PDMS surface with PVP, as described elsewhere [29]. Right after the plasma bonding, an aqueous solution of commercially available PVP 10% (w/w) was flowed through the two inlets with a syringe pump for 30 min. The channels were then flushed with distilled water and dried with compressed air. We used these functionalized chips right away, or after a few days, kept in air without noticing differences in their performance.

2.2. Liquids

Table 1 lists the main physical parameters of the liquids used in our study, as deduced from the literature [30,31] or measured directly. As a dispersed phase, we chose linseed oil, which we found perfectly compatible with the PDMS. As Newtonian continuous phases we chose two aqueous solutions of glycerol at concentrations of 60% and 85% (w/w). As non-Newtonian continuous phases we prepared aqueous solutions of xanthan (molecular weight, M_w ~10^6 g/mol, Sigma Aldrich) at three different concentrations 800 ppm, 1500 ppm and 2500 ppm (w/w). Their rheology was characterized with a parallel plate rheometer (Ares TA Instruments, New Castle, DE, USA). Figure 2 shows the measurements of the viscosity dependence on shear rate for the three solutions employed in this study. The viscosity μ_{Xan} is expected to vary with the shear rate $\dot{\theta}$ according to the power law $\mu_{Xan}(\dot{\theta}) = K\dot{\theta}^{(n-1)}$, where K is the flow consistency and n the flow behavior index, both dependent on the polymer concentration [32]. Table 2 shows the fitting parameters for the three solutions. Our data are in good agreement with the ones reported in [24] that explore a range of concentration and shear rate larger than the one accessible by our rheometer.

Table 1. Main physical properties of the liquids used in this study: density ρ, surface tension γ, dynamic viscosity μ (for xanthan solutions, the viscosity data correspond to a shear rate of 1 s^{-1}). All data refer to a temperature of 25 °C.

Liquid	ρ (g/cm^3)	γ (mN/m)	μ (mPa· s)
Linseed oil	0.93		22.3
Water	0.997	72	0.89
60% (w/w) Glycerol/Water	1.15	67.3	9
85% (w/w) Glycerol/Water	1.22	64.4	79
800 ppm (w/w) Xanthan/Water	0.997	72	76
1500 ppm (w/w) Xanthan/Water	0.997	72	312
2500 ppm (w/w) Xanthan/Water	0.997	72	985

Table 2. Fitting parameters of the power-law fit of the xanthan solutions.

Liquid	K (mPa· s^n)	n
800 ppm (w/w) Xanthan/Water	75.5 ± 0.6	0.491 ± 0.002
1500 ppm (w/w) Xanthan/Water	312.5 ± 1.6	0.389 ± 0.001
2500 ppm (w/w) Xanthan/Water	985 ± 6	0.302 ± 0.001

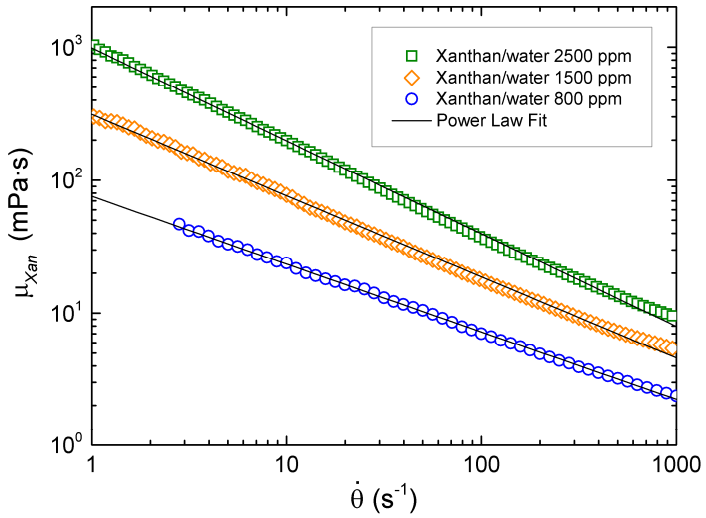

Figure 2. Viscosity characterization of xanthan solutions at different concentrations. Lines are $K\dot{\theta}^{(n-1)}$ fit to the data according to the power law fluid.

The interfacial tension between linseed oil and the various aqueous solutions used as continuous phase were measured with the pendant drop technique [33]. Pendant droplets of the aqueous solutions were made inside an oil filled cuvette, using a precision syringe with a stainless steel needle with an outer diameter of 210 µm. Pictures of the droplets were taken with collimated light and a telecentric objective. The droplets profiles were fitted with the axisymmetric solutions of the Young–Laplace equation to obtain the values of the surface tension of the liquid-liquid interface. The measured surface tensions are 10.1 ± 0.6 mN/m between water and linseed oil and 9.8 ± 0.4 mN/m between 85% (w/w) glycerol/water and linseed oil. The surface tensions between the xanthan aqueous solutions and linseed oil are the same as that between pure water and linseed oil due to the very low xanthan concentrations.

2.3. Imaging and Analysis

The droplet formation experiments were conducted in T-junction microfluidic chips with an overall size of 2 cm × 5 cm, see Figure 1. The microchannels had a width w = 120 µm and height h = 90 µm and were 2 cm long. Two independent syringe pumps (PHD 2000, Harvard Apparatus, Holliston, MA, USA) working at constant flow rates were used to introduce liquids into the microfluidic devices. Images of fully developed droplets were acquired far downstream the junction using a monochrome camera (EoSens® MC1362, Mikrotron, Unterschleißheim, Germany) coupled to an inverted microscope (Eclipse Ti-E, Nikon, Tokyo, Japan) at an acquisition rate up to 300 fps. Image processing and the measurement of droplets length were performed in real-time using a custom software written in LabView [34]. In this way, there was no need to store a huge amount of data and it was possible to accurately check that the droplet production reached stability after changing the flow rates. The images of Figure 1 shows some characteristic snapshots of different droplets formed at the T-junction and the characteristic frames analyzed by the program. The length L was then averaged over at least one hundred droplets for each flow rate. The polydispersity of the

emulsions was less than 2% at high flow rates of the continuous phase Q_c and less than 10% at the lowest Q_c.

3. Results and Discussion

3.1. Newtonian Droplets in a Newtonian Continuous Phase

Figure 3 summarizes the data concerning the production of oil droplets in a Newtonian matrix measured in functionalized PDMS chips. It shows the dimensionless droplet length, $\overline{L}$, defined as the time-averaged droplet length L normalized by the channel width w, as a function of the capillary number calculated for the continuous phase $Ca = \frac{\mu_c U_c}{\gamma} = \frac{\mu_c Q_c}{\gamma w h}$, where U_c is the average flow velocity of the continuous phase. The data refer to different ratios of the flow rates $\phi = Q_d/Q_c$ between the dispersed and continuous phases, indicated by different colors, spanning the range 0.1–0.8. The symbols instead represent three Newtonian aqueous solutions characterized by different viscosity ratios $\lambda = \mu_d/\mu_c$ between linseed oil (the dispersed phase) and the continuous phase: pure water ($\lambda = 25$), 60% (w/w) glycerol/water ($\lambda = 2.5$) and 85% (w/w) glycerol/water ($\lambda = 0.3$). In this way, the $\overline{L}$ data span a very ample interval of Ca (nearly four decades). At low flow rates ϕ, the data lie on a smooth line regardless of the viscosity ratio λ. Instead, at high ϕ the variation of the droplet length with the viscosity ratio λ becomes significant. Overall, the droplet length is found to decrease as the capillary number increases and to increase as the flow rate ratio increases. This trend is consistent with other studies where droplet production is controlled by two immiscible streams in a variety of different geometries [7,25,35].

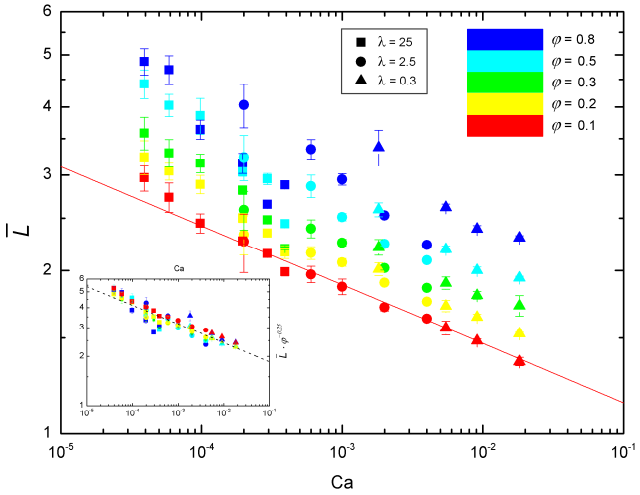

Figure 3. Dimensionless droplet length as a function of the capillary number of the continuous phase Ca for three aqueous solutions characterized by different viscosity ratios λ with the dispersed phase (linseed oil): $\lambda = 25$, water (full squares), $\lambda = 2.5$, 60% (w/w) glycerol/water (full dots), and $\lambda = 0.3$, 85% (w/w) glycerol/water (full triangles). The colors refer to different ratios of the flow rates ϕ. Inset: dimensionless droplet length, $\overline{L}$, normalized to $\phi^{0.25}$ as a function of Ca.

In the squeezing regime, *i.e.*, for $Ca \lesssim 0.01$, the length of the drops can be conveniently expressed with the following scaling equation $\overline{L} = \alpha_1 + \alpha_2 \frac{Q_d}{Q_c}$, where α_1 and α_2 are two constants of order one that depend on the junction geometry [10,36,37]. Accordingly, $\overline{L}$ should not depend on Ca if ϕ is constant. Instead, our measurements show no sign of approaching a constant value as the capillary number decreases. We find that, especially for the smallest ϕ values, the droplet length exhibits a power-law dependence on the capillary number $\overline{L} \propto Ca^{\beta}$, with $\beta = -0.109 \pm 0.003$ for $\phi = 0.1$, $\beta = -0.107 \pm 0.003$ for $\phi = 0.2$ and $\beta = -0.117 \pm 0.009$ for $\phi = 0.3$, in good agreement with

numerical results [38] and other experiments [35] spanning a narrower Ca interval. More interesting, the data are found to scale according to the formula $\overline{L} = k\varphi^{\alpha}\mathrm{Ca}^{\beta}$, where k is a constant whose value depends on the geometry of the T junction [36]. The inset of Figure 2 shows the dimensionless droplet length, $\overline{L}$, normalized to $\phi^{0.25}$ as a function of the capillary number of the continuous phase Ca. It is evident that the normalized droplet lengths nicely collapse on a straight line. The resulting scaling exponents, $\alpha = 0.25 \pm 0.05$ and $\beta = -0.120 \pm 0.004$ are in very good agreement with those originally found by Xu *et al.* in a narrower Ca range [36], $\alpha = 1/3$ and $\beta = -0.2$.

3.2. Newtonian Droplets in a Non-Newtonian Continuous Phase

We have repeated these measurements substituting the Newtonian aqueous solutions with those containing xanthan. Since the viscosity of the continuous phase now changes considerably (see next), the data have been plotted in terms of the ratio of the flow rates ϕ in the graph of Figure 4. It shows the variation of the droplet length for three xanthan solutions while keeping the flow rate of the continuous phase constant, $Q_c = 0.6$ μL/min. The data are compared with those obtained with a 85% (w/w) glycerol/water solution, whose viscosity is similar to the viscosity of 800 ppm (w/w) xanthan/water at low shear rates ($\dot{\theta} = 1\ \mathrm{s}^{-1}$), and with a 60% ($w/w$) glycerol/water solution whose viscosity is nine times smaller than the denser (85% (w/w) glycerol/water) one. The droplet length in glycerol solutions increases linearly with the flow rate of the dispersed phase $Q_d = Q_c\varphi$ as expected [10,25,35,36]. Instead, increasing the viscosity of the continuous phase produces shorter plugs [35,36,39], see also Figure 1. The lengths of oil droplets corresponding to 800 ppm (w/w) xanthan/water are significantly longer, about 30%, than those obtained with the 85% glycerol solution. However, they are very similar to the oil droplet lengths formed in the 60% glycerol solution. Increasing the xanthan concentration to 1500 ppm does not markedly affect the droplet length. A small decrease in $\overline{L}$, about 10%, is found at the highest xanthan concentration investigated, 2500 ppm. The data of Figure 4 suggest that the effective viscosity of the xanthan solutions when the T-junction is operating is much lower than the static one. Given the good agreement with the data corresponding to the solution 60% (w/w) glycerol/water, we can estimate that, at $Q_c = 0.6$ μL/min, the effective viscosity of the 800 ppm xanthan solution amounts to about 10 mPa·s, *i.e.*, it has decreased by a factor of approximately eight, with respect to its consistency value (*i.e.*, the viscosity measured at $\dot{\theta} = 1\ \mathrm{s}^{-1}$) value. This implies that the shear rates of this continuous phase during droplet breakup are on the order of 50 s^{-1}, as derived from the rheological data of Figure 2. Similar considerations hold for the other xanthan concentrations at different flow rates. For instance, if we consider a much higher continuous flow rate, $Q_c = 4$ μL/min, the length of oil droplets in presence of the 800 ppm xanthan solution is similar to that of oil in water. Therefore, the effective viscosity of the xanthan solution is now decreased by a factor ~80 and the corresponding shear rate increases to about 1000 s^{-1}.

To complete the characterization of the droplet formation in a shear-thinning medium, Figure 5 shows the average length of oil droplets as a function of the flow rate ratio of the 800 ppm (w/w) xanthan/water solution at constant flow rates Q_c. As in Figure 4, the droplet length increases almost linearly with the dispersed flow rate $Q_d = Q_c\varphi$. Furthermore, $\overline{L}$ decreases with increasing the continuous flow rate, again in agreement with the general trend found in Newtonian fluids [10,25,35,36]. The data corresponding to $Q_c = 0.2$ μL/min practically coincide with those obtained with the 60% (w/w) glycerol/water solution, confirming that also at this continuous flow rate the dynamic behavior of the 800 ppm xanthan solution in the T-junction is very similar to that of the 60% glycerol solution. However, increasing the flow rate of the xanthan solution to $Q_c = 2$ μL/min produces much longer plugs (about 15%) than those obtained with the 60% glycerol solution at the same Q_c, see also Figure 1. Again, this difference can be explained in terms of a variation of the viscosity of the xanthan solution with the continuous flow rate. Similar conclusions have been recently drawn analyzing the siding motion of xanthan droplets on a surface [40].

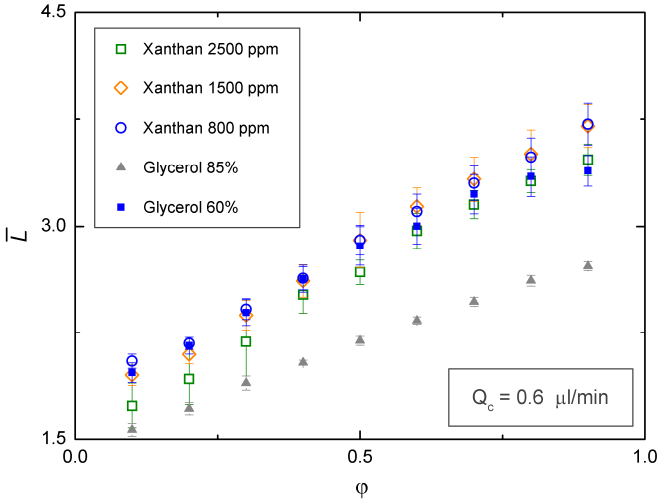

Figure 4. Dimensionless droplet length as a function of the flow rate ratio for three xanthan solutions characterized by different viscosity ratios λ with the dispersed phase (linseed oil). Xanthan 800 ppm λ = 0.3 (xanthan's value is the shear dependent viscosity measured at $\dot{\theta} = 1\ s^{-1}$), xanthan 1500 ppm λ = 0.07 and xanthan 2500 ppm λ = 0.023. As a comparison, we have also plotted the data of the Newtonian solutions 60% (*w*/*w*) glycerol/water (λ = 2.5) and 85% (*w*/*w*) glycerol/water (λ = 0.28). The results refer to a constant flow rate of the continuous phase Q_c = 0.6 µL/min.

From the scaling relation we have deduced from the Newtonian data, $\overline{L} \propto \varphi^{0.25} Ca^{-0.12}$, we can derive the ratio $\overline{L}_{G,0.2}/\overline{L}_{G,2}$ between the lengths of the oil plugs in the 60% glycerol solutions at the investigated extremes, Q_c = 0.2 µL/min and Q_c = 2 µL/min, in the case of a constant flow rate ratio ϕ. We find $\overline{L}_{G,0.2}/\overline{L}_{G,2} \sim 1.3$, in very good agreement with the experimental value of about 1.4 ± 0.15 at $\phi = 0.5$, a confirmation of the validity of the scaling law. If we assume that the same scaling holds for the xanthan solution, we obtain that $\overline{L}_{X,0.2}/\overline{L}_{X,2} = (0.2\mu_{X,0.2}/2\mu_{X,2})^{-0.12}$, where $\mu_{X,0.2}$ ($\mu_{X,2}$) represents the viscosity of the xanthan solution corresponding to a flow rate Q_c = 0.2 µL/min (Q_c = 2 µL/min). At ϕ = 0.5, the measured ratio of the droplets length in the 800 ppm xanthan solution is about 1.2. This implies that the viscosity of the xanthan solution drops from a factor of about 2.5 when its flow rate passes from 0.2 to 2 µL/min.

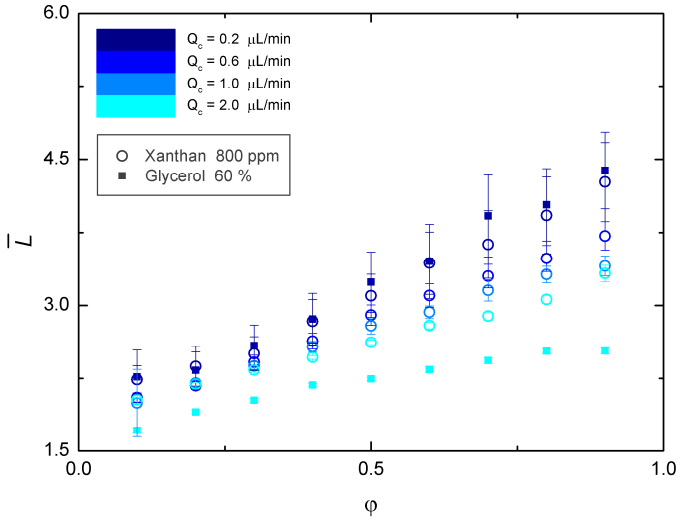

Figure 5. Dimensionless droplet length as a function of the flow rate ratio for the xanthan 800 ppm solution at constant Q_c (empty circles). As a comparison, we have also plotted the data of the Newtonian solution 60% (*w*/*w*) glycerol/water (full squares).

4. Conclusions

We have compared the formation of oil drops in Newtonian and non-Newtonian aqueous solutions using a T-junction device. The disposable microfluidic chips were made in PDMS and the microchannels walls were rendered hydrophilic after a surface treatment with PVP. This allowed the generation of oil droplets without the addition of any surfactant to the continuous phase. As Newtonian liquids we used aqueous solutions of glycerol. As non-Newtonian liquids we prepared aqueous solutions of xanthan that exhibit strong shear-thinning effects. In the squeezing regime, the formation of oil droplets in glycerol solutions is found to scale with the ratio of the dispersed flow rate to the continuous one and with the capillary number associated to the continuous phase. Switching to xanthan solutions does not seem to significantly change the break-up process. Any quantitative difference with respect to the Newtonian liquid can be accounted for by a suitable value of the xanthan viscosity that depends on the flow rates. We have deduced ample variations in the viscosity, on the order of 10 and more, during normal operation conditions of the T-junction. This allowed estimating the actual shear rates experienced by the xanthan solutions, which go from tens to hundreds of s^{-1}. Systematic measurements are in progress to investigate shear thinning effects on the squeezing to dripping transition. They will be also extended to polyacrylamide water solutions (PAA) that, at variance with xanthan solutions, feature normal stress difference effects. For a better understanding of these phenomena, it would be of great interest to complement the experimental observations with numerical simulations that allow to evaluate both the stress tensor and the distribution of the shear rate inside the T-junction, and to monitor the momentum balance equations for non-Newtonian fluids during the process of break-up. To this aim, generalization of the investigations we have proposed for sliding droplets [41,42] are surely warranted for future investigations.

Acknowledgments: Evandro Piccin acknowledges a Visiting Scholar fellowship from Università di Padova. Grants from European Research Council under the European Community's Seventh Framework Programme (FP7/2007-2013)/ERC Grant Agreement N. 297004 and from the Università di Padova (PRAT 2011 'MINET') are gratefully acknowledged. Finally, we are grateful to Laura Dal Toso for kind help in the data analysis and Professor Mauro Sbragaglia for fruitful discussions.

Author Contributions: Giampaolo Mistura and Matteo Pierno conceived the project. Enrico Chiarello and Evandro Piccin fabricated the chips and took the data. Ladislav Derzsi functionalized the PDMS chips. All authors contributed to the editing of the manuscript.

Conflicts of Interest: The authors declare no conflict of interest.

References

1. deMello, A.J. Control and detection of chemical reactions in microfluidic systems. *Nature* **2006**, *442*, 394–402. [CrossRef] [PubMed]
2. Teh, S.-Y.; Lin, R.; Hung, L.-H.; Lee, A.P. Droplet microfluidics. *Lab Chip* **2008**, *8*, 198–220. [CrossRef] [PubMed]
3. Theberge, A.B.; Courtois, F.; Schaerli, Y.; Fischlechner, M.; Abell, C.; Hollfelder, F.; Huck, W.T.S. Microdroplets in microfluidics: An evolving platform for discoveries in chemistry and biology. *Angew. Chem. Int. Ed.* **2010**, *49*, 5846–5868. [CrossRef] [PubMed]
4. Baroud, C.N.; Gallaire, F.; Dangla, R. Dynamics of microfluidic droplets. *Lab Chip* **2010**, *10*, 2032–2045. [CrossRef] [PubMed]
5. Seemann, R.; Brinkmann, M.; Pfohl, T.; Herminghaus, S. Droplet based microfluidics. *Rep. Prog. Phys.* **2012**, *75*, 016601. [CrossRef] [PubMed]
6. Elvira, K.S.; Solvas, X.C.I.; Wootton, R.C.R.; deMello, A.J. The past, present and potential for microfluidic reactor technology in chemical synthesis. *Nat. Chem.* **2013**, *5*, 905–915. [CrossRef] [PubMed]
7. Christopher, G.F.; Anna, S.L. Microfluidic methods for generating continuous droplet streams. *J. Phys. D Appl. Phys.* **2007**, *40*, R319–R336. [CrossRef]
8. Anna, S.L.; Bontoux, N.; Stone, H.A. Formation of dispersions using "flow focusing" in microchannels. *Appl. Phys. Lett.* **2003**, *82*, 364–366. [CrossRef]

9. Cramer, C.; Fischer, P.; Windhab, E.J. Drop formation in a co-flowing ambient fluid. *Chem. Eng. Sci.* **2004**, *59*, 3045–3058. [CrossRef]
10. Garstecki, P.; Fuerstman, M.J.; Stone, H.A.; Whitesides, G.M. Formation of droplets and bubbles in a microfluidic T-junction—Scaling and mechanism of break-up. *Lab Chip* **2006**, *6*, 437–446. [CrossRef] [PubMed]
11. Steinhaus, B.; Shen, A.Q.; Sureshkumar, R. Dynamics of viscoelastic fluid filaments in microfluidic devices. *Phys. Fluid.* **2007**, *19*, 073103. [CrossRef]
12. Arratia, P.E.; Gollub, J.P.; Durian, D.J. Polymeric filament thinning and breakup in microchannels. *Phys. Rev. E* **2008**, *77*, 036309. [CrossRef] [PubMed]
13. Arratia, P.E.; Cramer, L.A.; Gollub, J.P.; Durian, D.J. The effects of polymer molecular weight on filament thinning and drop breakup in microchannels. *New J. Phys.* **2009**, *11*, 115006. [CrossRef]
14. Derzsi, L.; Kasprzyk, M.; Plog, J.P.; Garstecki, P. Flow focusing with viscoelastic liquids. *Phys. Fluid.* **2013**, *25*, 092001. [CrossRef]
15. Thorsen, T.; Roberts, R.W.; Arnold, F.H.; Quake, S.R. Dynamic pattern formation in a vesicle-generating microfluidic device. *Phys. Rev. Lett.* **2001**, *86*, 4163–4166. [CrossRef] [PubMed]
16. Husny, J.; Cooper-White, J.J. The effect of elasticity on drop creation in T-shaped microchannels. *J. Non Newton. Fluid Mech.* **2006**, *137*, 121–136. [CrossRef]
17. Christopher, G.F.; Anna, S.L. Passive breakup of viscoelastic droplets and filament self-thinning at a microfluidic T-junction. *J. Rheol.* **2009**, *53*, 663–683. [CrossRef]
18. Gu, Z.; Liow, J.-L.; Zhu, G. Investigation on the droplet formation time with xanthan gum solutions at a T-junction. In Proceedings of the ASME 2012 Fluids Engineering Division Summer Meeting, Rio Grande, PR, USA, 8–12 July 2012; Volume 2, pp. 299–307.
19. Li, X.B.; Li, F.C.; Kinoshita, H.; Oishi, M.; Oshima, M. Dynamics of viscoelastic fluid droplet under very low interfacial tension in a serpentine T-junction microchannel. *Microfluid. Nanofluid.* **2015**, *18*, 1007–1021. [CrossRef]
20. Gupta, A.; Sbragaglia, M. Deformation and breakup of viscoelastic droplets in confined shear flow. *Phys. Rev. E* **2014**, *90*, 023305. [CrossRef] [PubMed]
21. Whitcomb, P.; Macosko, C. Rheology of xanthan gum. *J. Rheol.* **1978**, *22*, 493–505. [CrossRef]
22. Zirnsak, M.A.; Boger, D.V.; Tirtaatmadja, V. Steady shear and dynamic rheological properties of xanthan gum solutions in viscous solvents. *J. Rheol.* **1999**, *43*, 627–650. [CrossRef]
23. Carre, A.; Eustache, F. Spreading kinetics of shear-thinning fluids in wetting and dewetting modes. *Langmuir* **2000**, *16*, 2936–2941. [CrossRef]
24. Rafai, S.; Bonn, D.; Boudaoud, A. Spreading of non-Newtonian fluids on hydrophilic surfaces. *J. Fluid Mech.* **2004**, *513*, 77–85. [CrossRef]
25. Piccin, E.; Ferraro, D.; Sartori, P.; Chiarello, E.; Pierno, M.; Mistura, G. Generation of water-in-oil and oil-in-water microdroplets in polyester-toner microfluidic devices. *Sens. Actuators B Chem.* **2014**, *196*, 525–531. [CrossRef]
26. Brigo, L.; Carofiglio, T.; Fregonese, C.; Meneguzzi, F.; Mistura, G.; Natali, M.; Tonellato, U. An optical sensor for pH supported onto tentagel resin beads. *Sens. Actuators B Chem.* **2008**, *130*, 477–482. [CrossRef]
27. Silvestrini, S.; Ferraro, D.; Toth, T.; Pierno, M.; Carofiglio, T.; Mistura, G.; Maggini, M. Tailoring the wetting properties of thiolene microfluidic materials. *Lab Chip* **2012**, *12*, 4041–4043. [CrossRef] [PubMed]
28. Glawdel, T.; Ren, C.L. Droplet formation in microfluidic T-junction generators operating in the transitional regime. III. Dynamic surfactant effects. *Phys. Rev. E* **2012**, *86*, 026308. [CrossRef] [PubMed]
29. Hemmila, S.; Cauich-Rodriguez, J.V.; Kreutzer, J.; Kallio, P. Rapid, simple, and cost-effective treatments to achieve long-term hydrophilic PDMS surfaces. *Appl. Surf. Sci.* **2012**, *258*, 9864–9875. [CrossRef]
30. Mirabedini, S.M.; Dutil, I.; Farnood, R.R. Preparation and characterization of ethyl cellulose-based core-shell microcapsules containing plant oils. *Colloids Surf. A Phys. Eng. Asp.* **2012**, *394*, 74–84. [CrossRef]
31. Glycerine Producers' Association. *Physical Properties of Glycerine and Its Solutions*; Glycerine Producers' Association: New York, NY, USA, 1963.
32. Macosko, C.W. *Rheology: Principles, Measurements, and Applications*; Wiley-VCH: Weinheim, Germany, 1994.
33. Hoorfar, M.; Neumann, A.W. Recent progress in Axisymmetric Drop Shape Analysis (ADSA). *Adv. Colloid Interf. Sci.* **2006**, *121*, 25–49. [CrossRef] [PubMed]

34. Ferraro, D.; Semprebon, C.; Toth, T.; Locatelli, E.; Pierno, M.; Mistura, G.; Brinkmann, M. Morphological transitions of droplets wetting rectangular domains. *Langmuir* **2012**, *28*, 13919–13923. [CrossRef] [PubMed]
35. Christopher, G.F.; Noharuddin, N.N.; Taylor, J.A.; Anna, S.L. Experimental observations of the squeezing-to-dripping transition in T-shaped microfluidic junctions. *Phys. Rev. E* **2008**, *78*, 036317. [CrossRef] [PubMed]
36. Xu, J.H.; Li, S.W.; Tan, J.; Luo, G.S. Correlations of droplet formation in T-junction microfluidic devices: from squeezing to dripping. *Microfluid. Nanofluid.* **2008**, *5*, 711–717. [CrossRef]
37. Gupta, A.; Kumar, R. Effect of geometry on droplet formation in the squeezing regime in a microfluidic T-junction. *Microfluid. Nanofluid.* **2010**, *8*, 799–812. [CrossRef]
38. De Menech, M.; Garstecki, P.; Jousse, F.; Stone, H.A. Transition from squeezing to dripping in a microfluidic T-shaped junction. *J. Fluid Mech.* **2008**, *595*, 141–161. [CrossRef]
39. Xu, J.H.; Li, S.W.; Tan, J.; Wang, Y.J.; Luo, G.S. Preparation of highly monodisperse droplet in a T-junction microfluidic device. *AIChE J.* **2006**, *52*, 3005–3010. [CrossRef]
40. Varagnolo, S.; Mistura, G.; Pierno, M.; Sbragaglia, M. Sliding droplets of xanthan solutions: A joint experimental and numerical study. *Eur. Phys. J. E* **2015**, *38*, 126.
41. Varagnolo, S.; Ferraro, D.; Fantinel, P.; Pierno, M.; Mistura, G.; Amati, G.; Biferale, L.; Sbragaglia, M. Stick-slip sliding of water drops on chemically heterogeneous surfaces. *Phys. Rev. Lett.* **2013**, *111*, 066101. [CrossRef] [PubMed]
42. Sbragaglia, M.; Biferale, L.; Amati, G.; Varagnolo, S.; Ferraro, D.; Mistura, G.; Pierno, M. Sliding drops across alternating hydrophobic and hydrophilic stripes. *Phys. Rev. E* **2014**, *89*, 012406. [CrossRef] [PubMed]